Project on AC corrosion conducted at:
Department of Manufacturing Engineering, Materials Technology, Building 204,
The Technical University of Denmark, DK-2800 Lyngby, Denmark

Funded by:
DONG Natural Gas A/S. Agern Allé 24-26, DK-2970 Hørsholm, Denmark.

June 2000

EIS Investigation of the Randles Circuit Elements for Carbon Steel Exposed in Artificial Soil Solution.

Lars Vendelbo Nielsen
lvn@ipt.dtu.dk

Keywords:
Electrochemical Impedance Spectroscopy (EIS), DC-offset potential, area effects, spread resistance, polarisation resistance, capacitance

Abstract

This paper describes observations on the pH- and potential profile evolving from a cathodically protected steel surface buried in a sand-sediment saturated with synthetic soil solution. It is shown that an alkalisation front (pH = 11) develops from the surface, and after some 20 days of CP, the front reaches 50 cm into the sediment. From chemical equilibrium considerations and IR-drop calculations, it is shown that the produced OH^- reacts first with Mg^{2+} (not Ca^{2+})- ions after which proceeds a release of ionic hydroxide leading to the alkalisation. OCP-measurements on steel plates inserted into the resulting pH profile show an expected dependency on pH.

Introduction

Using electrochemical impedance spectroscopy (EIS) as a tool in corrosion studies generally requires an electrical equivalent model representing the corrosion process in order to interpret the EIS data. The most simple equivalent circuit is the Randles circuit, consisting of :

- An ohmic resistance R_s across which the well-known IR-drop occurs when making potential measurements with a reference electrode placed some distance away from the sample under conditions involving an external current flowing to said sample.
- A polarisation resistance R_p describing the sum of the resistances towards charge transfer of all charge-transfer controlled electrochemical processes active during the measurement.
- An interfacial capacitance C placed in parallel with R_{ct} describing the capacitive feature of the interface between the sample and the surrounding solution.

The simple Randles circuit is shown in figure 1(a).

If diffusion provides some limitation of the access of species to (or transport away from) the surface of the sample at which the processes occur, a diffusion element in the form of a Warburg impedance is often inserted in series with the charge transfer resistance (figure 1(b)).

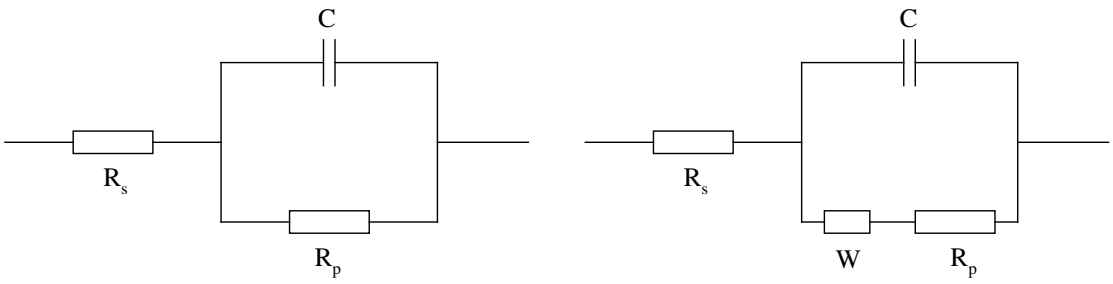

Figure 1. The Randles circuit (a) and the Randles circuit extended with a Warburg diffusion element.

The aim of the present investigation were to apply the EIS technique on steel samples of varying area exposed in an artificial soil solution, hereby to investigate the effect of the DC offset potential as well as the sample area on the quantities represented in particular by the simple Randles circuit.

Experimental

Electrodes with various active areas were made by painting Ø10 x 10 mm cylindrical mild steel (St-37) samples on part of the area, hereby leaving the desired active surface area unpainted as illustrated in figure 2. The following active areas were produced: 0.01, 0.1, 0.4, 1, and 4 cm^2. 8 electrodes were produces per area, in all 40 electrodes.

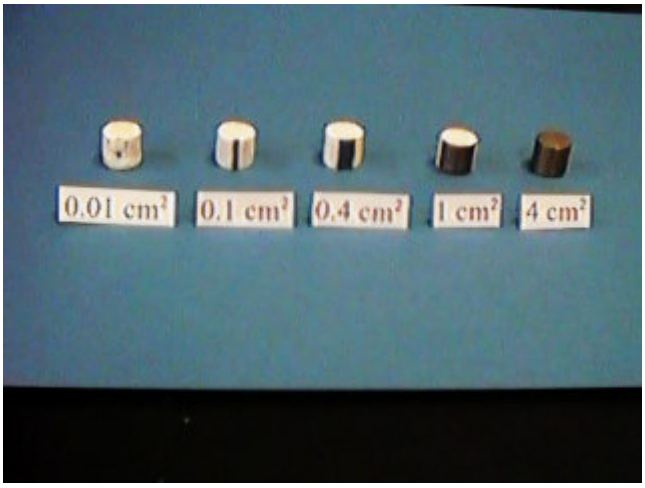

Figure 2. Specific areas provided by painting Ø10 x 10-mm cylindrical electrodes.

The electrodes were used as working electrodes in a traditional three-electrode set-up. A titanium mesh (Ø8 x 6 cm) surrounding the working electrode acted as the counter electrode, and a saturated calomel electrode (E_{SCE} = 242 mV SHE) placed in a Luggin capillary was used as reference electrode. It was ensured that the Luggin capillary was placed in the same location relative to the active area during all experiments.

Artificial soil solution with the chemical composition according to table 1 was used as electrolyte in all experiments. The solution was purged with nitrogen gas.

Component	Concentration (mg/L)	Concentration (mol/L)
$MgSO_4$, $7H_2O$	617	$2.5 \cdot 10^{-3}$
$CaSO_4$, $2H_2O$	430	$2.5 \cdot 10^{-3}$
$NaHCO_3$	210	$2.5 \cdot 10^{-3}$
$CaCl_2$	554	$5.0 \cdot 10^{-3}$

Table 1. Chemical composition of the artificial soil solution. The resulting pH was approximately 7.8.

For each electrode area, EIS measurements were performed at the following DC-offset "on"-potentials (mV versus SCE): -1000, -850, -700, -650, -600,-500, -200, as well as at the open circuit potential. Each measurement was performed according to the following schedule:

1. A fresh amount of artificial soil solution was transferred to the cell and de-oxygenated by purging with N_2.

2. The electrode was mounted in the cell and allowed to stabilise at the selected DC-offset potential for 15 minutes.

3. EIS measurements were made using the Gamry system (PC4 potentiostat controlled by CMS300 EIS software). A 10 mV perturbation was applied across the DC-offset in the frequency region 0.01 – 10000 Hz. During the measurements, the DC-potential and –current was recorded.

Results and discussion

The distinct quantities (R_s, R_p, C) were depicted according to common practice from the Nyquist plot (imaginary versus real part impedance) and Bode plot (total electrode impedance and phase angle as a function of frequency) as shown in figure 3, and further explained throughout the discussion.

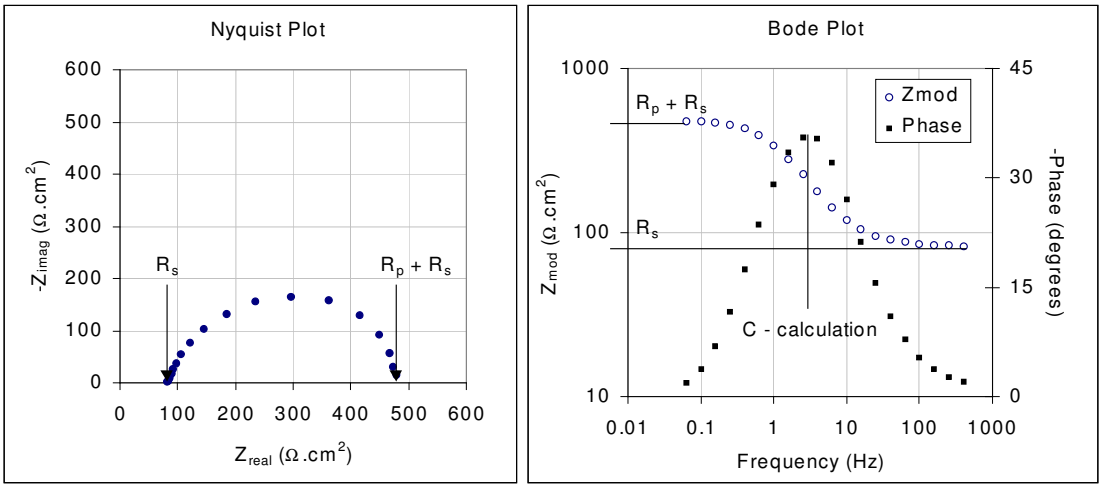

Figure 3. Illustration of Nyquist- and Bode plot resulting from EIS-measurement, and how to depict the simple quantities of interest.

Initially, the individual Randles circuit elements estimated by the EIS measurements are presented and discussed. Hereafter, some general considerations on the correlation between DC-polarisation behaviour and the EIS-measurements are offered.

Ohmic resistance, R_s.

The ohmic resistance is determined as the real part impedance occurring at the high frequency part of the measurements. It may be established from either the Nyquist- or the Bode plot. Table 2 outlines the absolute R_s-values determined for the different electrode areas and offset potentials.

R_s Ω	-1000 mV	-850 mV	-700 mV	-650 mV	OCP	-600 mV	-500 mV	-200 mV	**Average**
0.01 cm^2	1200	1200	2000	1500	1500	1500	1500	500	**1362**
0.1 cm^2	600	500	500	400	400	400	400	230	**428**
0.4 cm^2	350	250	250	275	200	250	275	190	**255**
1.0 cm^2	200	165	-	160	135	170	160	150	**162**
4.0 cm^2	63	61	61	63	60	70	68	61	**63**

Table 2. Ohmic resistance (absolute) obtained for the various electrode areas and offset potentials.

As observed from figure 4 (graphic illustration of the data from table 2), the absolute ohmic resistance decreases with increasing area as expected. A further illustration of this is given in figure 5 where the data from all experiments are presented directly as a function of the area.

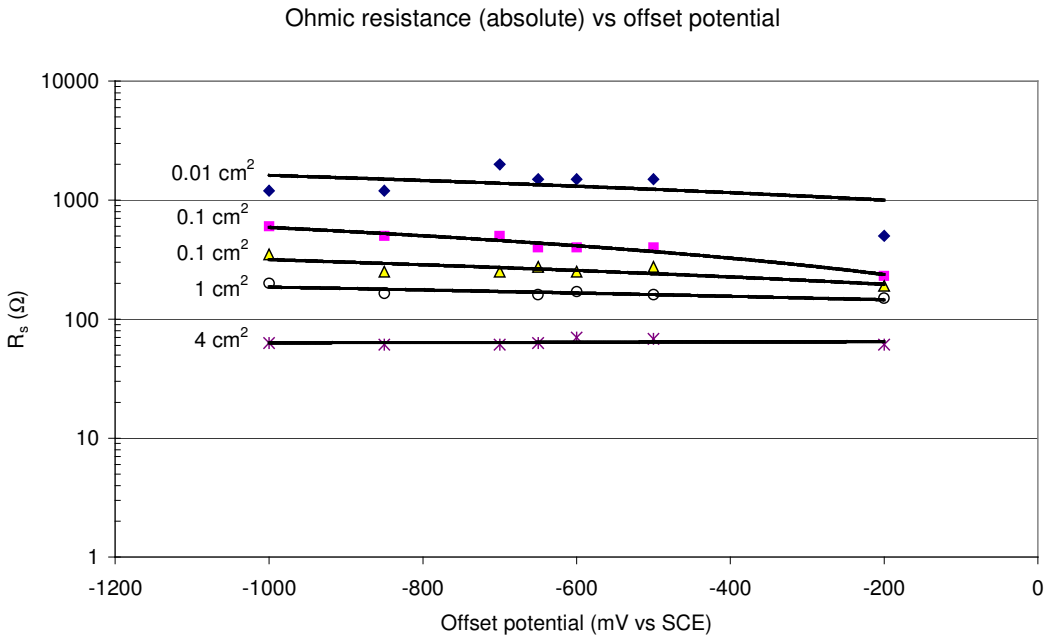

Figure 4. Absolute ohmic resistance versus offset potential for each electrode area.

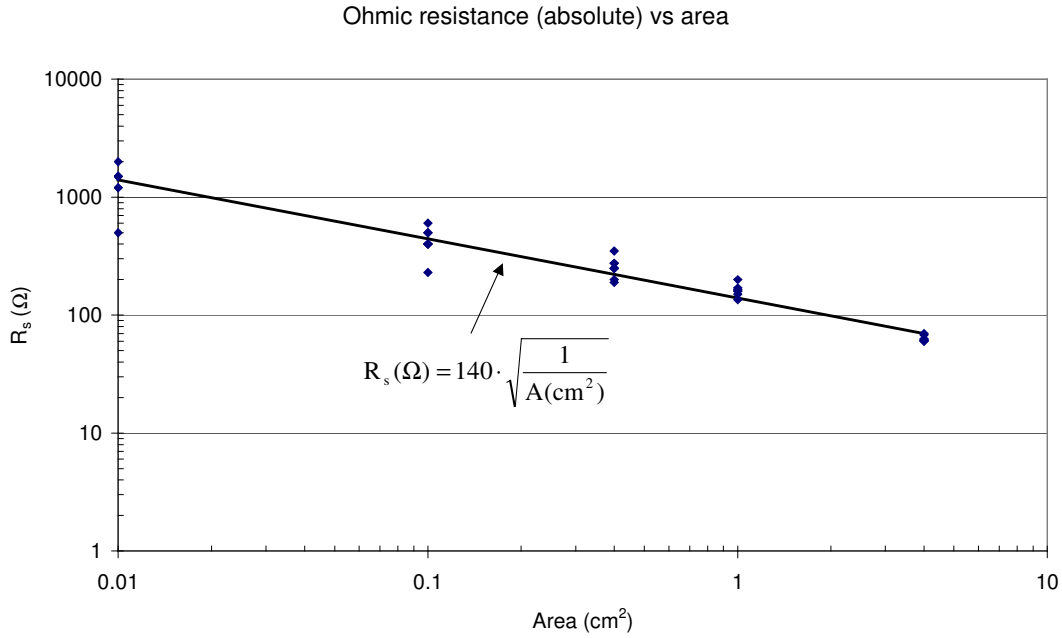

Figure 5. Absolute ohmic resistance as a function of the electrode area.

In figure 5, a line has been drawn representing the equation:

$$R_s(\Omega) = 140 \cdot \frac{1}{\sqrt{A(cm^2)}} \tag{1}$$

For comparison, the spread resistance ("ausbreitungwiderstand") for a hemispheric anode can be expressed as (according to "Handbuch des katodischen Korrosionnschutzes"[1]):

$$R = \frac{\rho}{\pi \cdot d} \tag{2}$$

where d is the diameter of the hemisphere, and ρ is the specific resistivity of the solution. The analogy between (1) and (2) is straightforward, since the area A is proportional to the square of the diameter d, and is taken as a justification of the experimental results.

Usually the ohmic resistance is normalised with respect to electrode area by multiplying with said area. Doing this, the values presented in table 3 are obtained.

R_s $\Omega.cm^2$	-1000 mV	-850 mV	-700 mV	-650 mV	OCP	-600 mV	-500 mV	-200 mV	**Average**
0.01 cm^2	12	12	20	15	15	15	15	5	**14**
0.1 cm^2	60	50	50	40	40	40	40	23	**43**
0.4 cm^2	140	100	100	110	80	100	110	76	**102**
1.0 cm^2	200	165	-	160	135	170	160	150	**163**
4.0 cm^2	252	244	244	252	240	280	272	244	**254**

Table 3. Ohmic resistance (normalised) obtained for the various electrode areas and offset potentials.

Again, these data can be plotted as a function of the area (figure 6), now fitting quite well into the equation:

$$R_s(\Omega \cdot cm^2) = 140 \cdot \sqrt{A(cm^2)} \qquad (3)$$

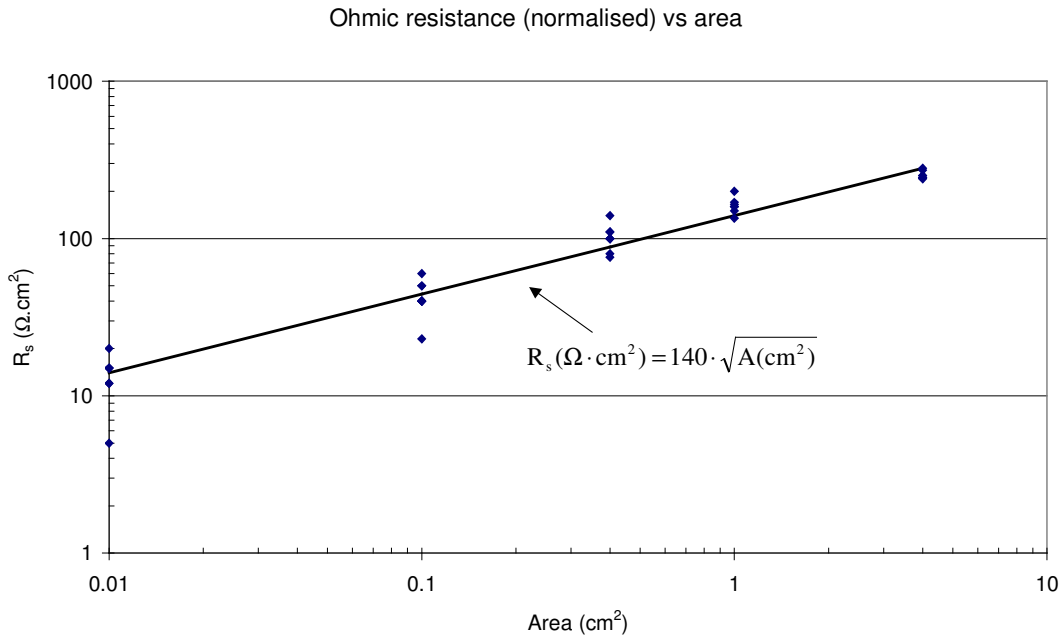

Figure 6. The normalised ohmic resistance as a function of electrode area.

In relation to equation (1) and (2), equation (3) can be somewhat justified using dimension analysis (assuming the electrode area to be a square with side length d).

The important consequence of equation (3) is that the IR-drop occurring at small defects in a pipeline coating is considerably smaller than the IR-drop that is occurring at larger coating defects.

Polarisation resistance, R_p.

The determination of the polarisation resistance is somewhat more complicated than establishing the solution resistance. Figure 7 illustrates the characteristic EIS plots obtained as a function of the DC offset potentials for the 0.1 cm^2 electrode. With reference to this figure, it is observed that at the open circuit potential (OCP), the Nyquist plot exhibit a quite perfect semicircle, from which the polarisation resistance is easily obtained as the chord that cuts of the real part axis (as pointed out in figure 3). At more cathodic potentials, the semicircle becomes increasingly less completed, indicating effects of diffusion. The clear sign of a second semicircle at –1000 mV may indicate precipitation of solids. At potentials that are more anodic relative to the OCP, the semicircle seems to bend over in the low frequency end, which may indicate that the active surface area increases during the measurement (decreasing the polarisation resistance) due to metal dissolution. These observations are sustained by observing the phase angle versus frequency behaviour. Ideally, this should be symmetrical around the minimum point. When diffusion dominates the low frequency part, the curve broadens out at these frequencies. Contrary, when the electrode area increases due to metal dissolution, the curves becomes steeper in the low frequency end.

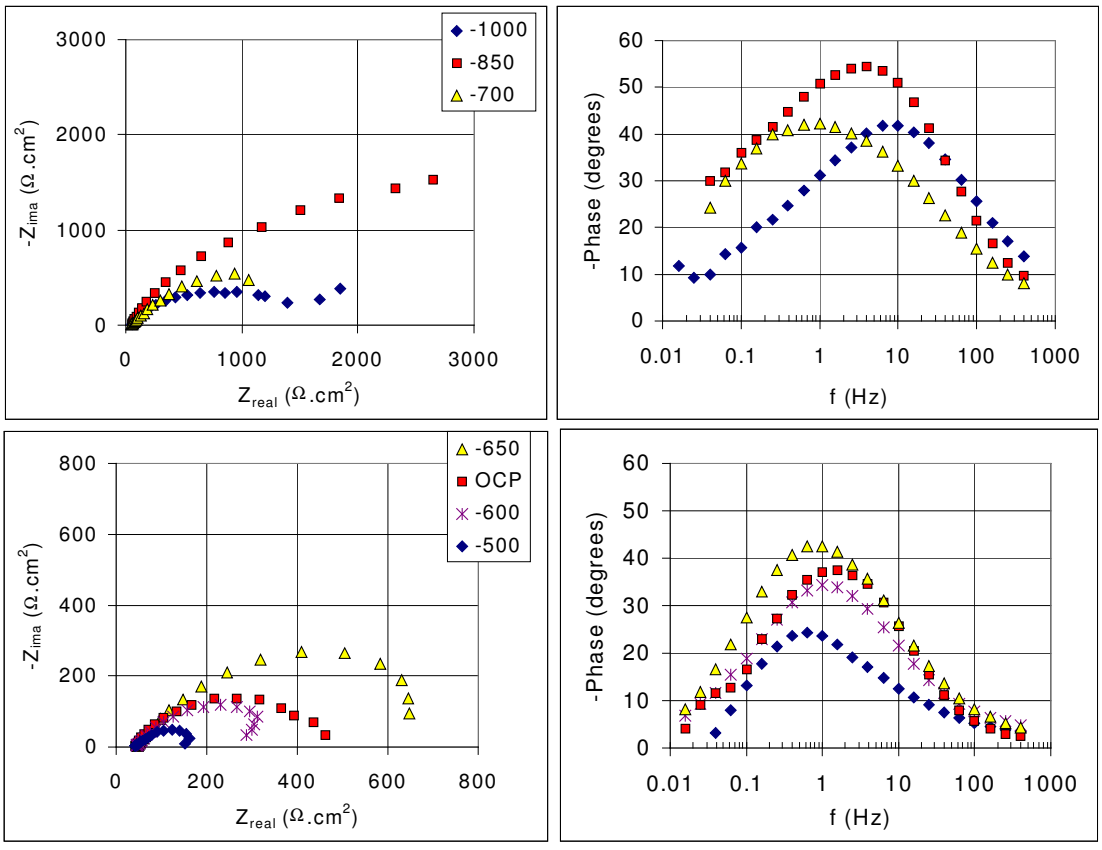

Figure 7. Characteristic EIS plots obtained at different potentials for the 0.1 cm2 electrode. Left: Nyquist plots. Right: Bode plots (only phase angles included). Upper: Cathodic DC polarisation potentials including the OCP, Lower: anodic DC polarisation potentials.

The above remarks set up some limitations regarding the estimation of the polarisation resistance. If the semicircle is not completed or easily extrapolated to the real part axis at low frequencies, the estimate is made as "$R_p > X$", where X is an estimate for R_p which – based on the curve behaviour – does not exceed the true R_p. Table 4 outlines the R_p estimates. The values have been normalised with respect to the surface area, i.e. given in $\Omega \cdot cm^2$. The data are related to the offset conditions in a later section of the paper.

R_p $\Omega \cdot cm^2$	-1000 mV	-850 mV	-700 mV	-650 mV	OCP	-600 mV	-500 mV	-200 mV
0.01 cm^2	>100	>250	>750	200	90	180	1150	1
0.1 cm^2	>2000	>4000	1200	610	420	220	110	5
0.4 cm^2	>3000	>8000	>6000	1150	390	>2000	400	10
1.0 cm^2	>5000	>7000	-	1250	550	>3000	2000	15
4.0 cm^2	4000	-	3000	>7000	600	7000	830	15

Table 4. Estimate of normalised polarisation resistance in relation to electrode area and offset potential.

Electrode capacitance, C.

The electrode capacitance, C, is usually estimated from the equation:

$$C = \frac{1}{2 \cdot \pi \cdot f_{\varphi min} \cdot Z_{\varphi min}} \tag{4}$$

where $f_{\varphi min}$ is the frequency at which the phase angle is at its minimum (the extremum point, i.e. numerically the maximum phase according to figure 3), and $Z_{\varphi min}$ is the impedance at this frequency. However, by using this equation, it is assumed that $R_p >> R_s$, otherwise the estimate becomes wrong. In this investigation, the condition $R_p >> R_s$ definitely does not exist in measurements performed at the DC offset potential = -200 mV where the polarisation resistance is low. Other offset potentials provide to some extent the same deviation from the condition $R_p >> R_s$. Control measurements using real electrical components substituting R_s, R_p, and C were conducted showing that when the condition Rp>>Rs was not fulfilled, the following equation gives a more accurate estimate:

$$C = \frac{1}{2 \cdot \pi \cdot f_{\varphi min} \cdot Z_{\varphi min}} \cdot \frac{R_s + R_p}{R_p} \tag{5}$$

This equation involves exact knowledge of R_p, and as mentioned previously, this is not obtainable when diffusion effects prohibits a completion of the semicircle in the Nyquist plot. However, when diffusion is predominating, the condition $R_p >> R_s$ generally exists, hence, equation (4) can be used to calculated the electrode capacitance.

Using the above concept, the following electrode capacitances (normalised with respect to electrode area) were been estimated:

C **µF /cm²**	-1000 mV	-850 mV	-700 mV	-650 mV	OCP	-600 mV	-500 mV	-200 mV
0.01 cm^2	115	110	125	1450	4130	760	45	1100
0.1 cm^2	95	130	640	800	770	1230	3500	370
0.4 cm^2	50	60	10	280	340	2630	1030	110
1.0 cm^2	70	55	-	120	260	170	180	110
4.0 cm^2	110	180	340	100	125	35	170	1125

Table 5. Capacitance estimations in relation to electrode area and offset potential..

These capacitance estimations seem to be difficult to interpret. However, a general observation is that around the OCP, the capacitance clearly decreases with increasing surface area, but no additional systematic behaviour is obvious. It is noted in this context that the electrode roughness, hence the preparation of the electrode surface, filming capacities as well as corrosion conditions may be in control of the capacitance, however, such factors play a role regarding the polarisation resistance and ohmic resistance as well.

Offset conditions

As mentioned previously, the EIS equipment is capable of recording the offset conditions (E_{DC}, I_{DC}) during the measurement. Attempting to establish a picture of the DC-polarisation behaviour the offset potential has to be cleaned from IR-drop, hereby establishing the OFF-potential E_{OFF} according to the equation:

$$E_{OFF} = E_{ON} - i_{DC} \cdot R_s \qquad (6)$$

where E_{ON} is the programmed offset potential, i_{DC} is the density of current flowing for frequency $f \rightarrow 0$, and R_s is the ohmic resistance. The resulting curves are assembled in figure 8. As observed, the curves do not appear as perfect Tafel polarisation curves. One reason undoubtedly is an overshoot of the IR-drop estimation in particular in the anodic region caused by severe corrosion (production of ferrous ions decreasing the ohmic resistance) taking place in the low frequency part of the EIS measurement. However, in particular in potential regions far from the open circuit potential (OCP) there is a tendency of increased current density with decreasing electrode area.

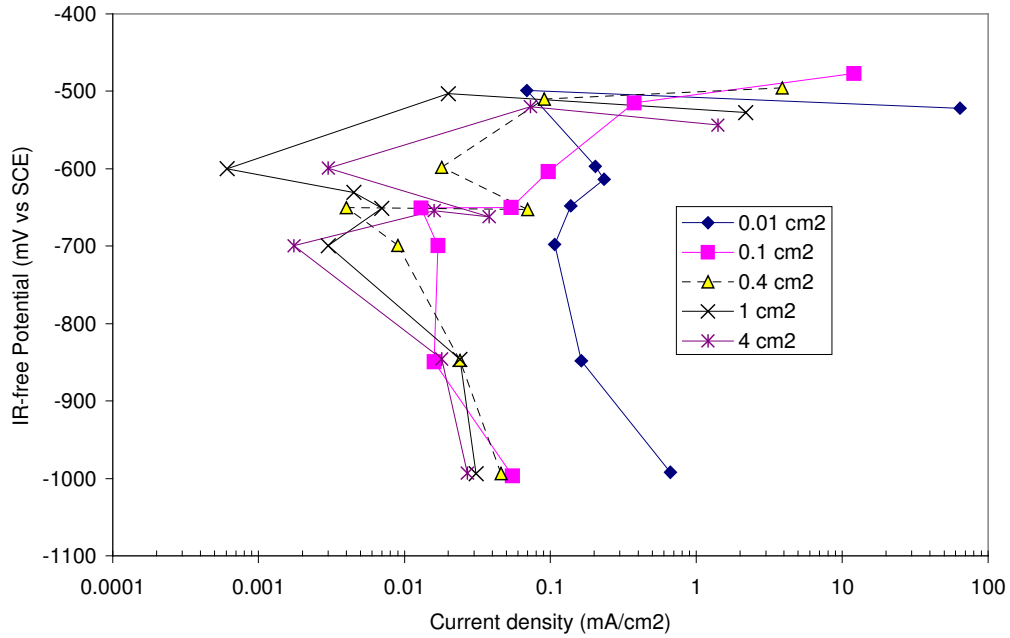

Figure 8. E_{OFF} - log(i_{DC}) behaviour established from the measurements for $f \rightarrow 0$. .

Another way of regarding the data is to compare e.g. the current density in the anodic region of the curves with the measured polarisation resistance. A modified Stearn-Geary equation can be applied to predict a possible behaviour:

$$R_p = \frac{R \cdot T}{n \cdot F} \cdot \frac{1}{i_{DC}} \qquad (7)$$

where R is the gas constant, T is the temperature in Kelvin, n is the number of electrons participating in the anodic dissolution process, and i_{DC} is the anodic (metal dissolution) current density. The equation suggests that a plot of R_p versus $1/I_{corr}$ should produce a straight line with slope = RT/nF (= 0.026 for n = 1). Figure 9 shows actual data obtained for all experiments at offset potential –500 mV and –200 mV (SCE). For comparison, the "theoretical" line is included showing a fair correlation, and the anodic behaviour of the electrodes may be part of the same curve, differing only in their OFF-potentials (at identical ON-potentials).

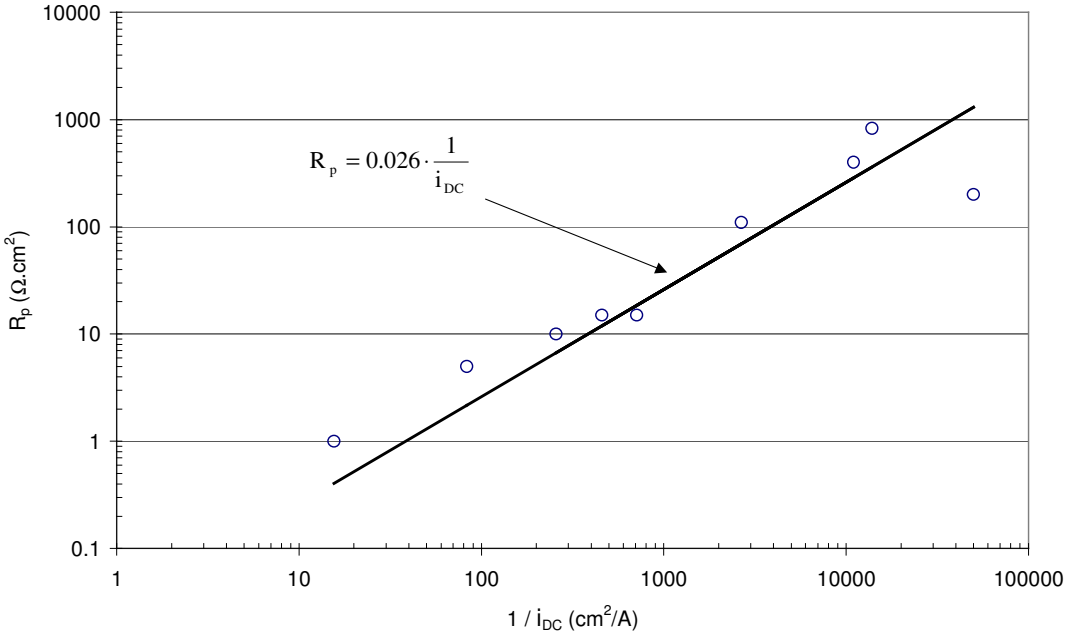

Figure 9. Polarisation resistance versus inverse anodic DC current. All experiments, anodic conditions (E = –200 and –500 mV SCE).

The cathodic behaviour of the electrodes differs from each other as observed from figure 8. The diffusion limited current density increases with decreasing area, hence, the electrodes do not share the same cathode branch. The explanation for this diversity has to be related to the diffusion conditions.

For linear diffusion to a completely flat electrode surface of infinite dimensions, it is only necessary to consider concentration differences and hence diffusion perpendicular to the electrode surface. The limiting current density in this simple case can be described by Fick's 1st law of diffusion:[2]

$$i = -n \cdot F \cdot D \cdot \frac{C_{bulk}}{\delta} \tag{8}$$

where i is the limiting current flowing to the electrode, D is the diffusion coefficient, C_{bulk} is the bulk concentration of the diffusing species, and δ is the extension of the diffusion layer. This means that for a certain constant bulk concentration, the limiting current is inversely related to the extension of the diffusion layer, δ. Regarding spherical diffusion, the limiting current density can be described by:[2]

$$i = -n \cdot F \cdot D \cdot \frac{C_{bulk}}{r} \tag{9}$$

where r is the radius of the electrode. A rough approximation of this equation to the electrode geometries used in the present investigation would be that instead of the electrode radius, r, the square root of the electrode area A multiplied by a constant K could be applied:

$$i = -n \cdot F \cdot D \cdot \frac{C_{bulk}}{\sqrt{K \cdot A}} \qquad (10)$$

This equation predicts that a plot of the limiting current density versus the inverse of the square root of the electrode area should produce a straight line. Applying actual data at e.g. –1000 mV SCE, the plot is not quite definitive (figure 10), but – if a more accurate and well-defined painting of the electrodes (figure 2) were observed, the above diffusion equations may have been justified more thoroughly.

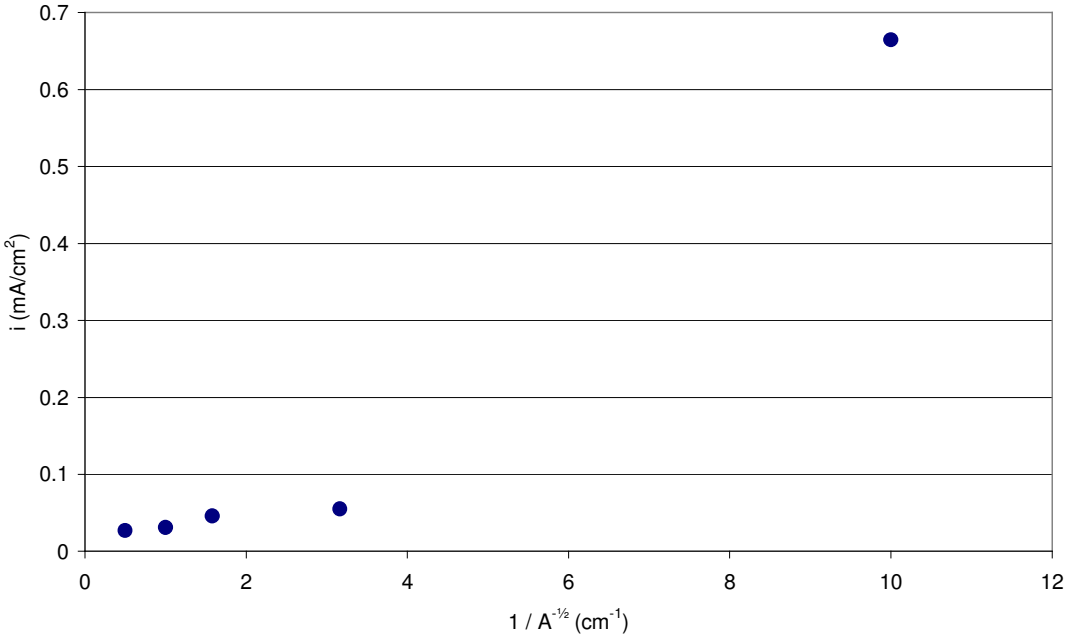

Figure 10. Cathodic current density at –1000 mV SCE versus square root of the inverse area.

Diffusion is defined as a random movement of species causing a flux of the species downhill a concentration gradient. Whenever such concentration gradient exists, diffusion occurs. Dealing with a coating defect, at which species are consumed or produced, the species diffuse in the direction with the lowest concentration. Regarding cathodically protected steel, the cathodic polarisation of the steel causes a displacement of the pH in the direction of alkalinity (rising pH), since the CP initiates cathode reactions like reduction of acid (5) or reduction of oxygen (6). As observed from these equations, acid (H^+) is consumed or alkalinity (OH^-) produced both causing a rise in pH corresponding a direct proportionality between the DC-current flow (e^-) and the produced equivalent of alkalinity. Since these reactions take place directly at the steel surface, this sets up a pH gradient (H^+ concentration gradient) in the proximity of the surface, and consequently diffusion processes initiate. Hence, diffusion processes renew H^+ at the cathodically protected surface, whereas OH^- diffuses away from the surface, both causing a moderation of the pH increase otherwise taking place at the surface.

The same scenario sets up when steel is corroding according to equation (4). In this case Fe^{2+} ions diffuses away from the surface.

Ficks' laws of diffusion determine the rate by which diffusion occurs:

$$1^{st}\text{ law of diffusion}: \qquad J_i = -D_i \cdot \frac{\delta C_i}{\delta x} \tag{18}$$

$$2^{nd}\text{ law of diffusion}: \qquad \frac{\delta C_i(x,t)}{\delta t} = D_i \cdot \frac{\delta^2 C_i(x,t)}{\delta x^2} \tag{19}$$

The first law states that the flux of the diffusing species J_i is proportional to the concentration gradient $\delta C_i/\delta x$, with the proportionality factor D_i (diffusion coefficient D_i). Note the analogy to Ohm's law (J_i ~ current I, $\delta C_i/\delta x$ ~ voltage U, and D_i ~ inverse resistance 1/R). The second law takes into account the effect of time changing gradients.

In figure 1, the diffusion element has been implemented as a Warburg impedance element, W, which is known from general electrochemical modelling. The magnitude of the impedance Z_D of such diffusion element can be described by the generic expression (originally a complex impedance with symmetrical coefficients):[2]

$$Z_D = \frac{\sigma}{\sqrt{\pi \cdot f}} \tag{20}$$

where σ, the Warburg coefficient is given by:

$$\sigma = \frac{R \cdot T}{n^2 \cdot F^2 \cdot A \cdot \sqrt{2}} \cdot \left(\frac{1}{C_{O,bulk} \cdot \sqrt{D_O}} + \frac{1}{C_{R,bulk} \cdot \sqrt{D_R}} \right) \tag{21}$$

R is the gas constant, T is temperature, n is number of electrons involved in the electrochemical process, F is Faraday's number, A is the area (of the coating defect), $C_{O,bulk}$ and $C_{R,bulk}$ is the bulk concentration of oxidant and reductant respectively, and D_O and D_R is related diffusion coefficients.

3.2 Effect of Diffusion

Firstly, it is noted that the Warburg coefficient (equation (21)) is inversely related to the surface area. Consequently the diffusion impedance (equation (20)) is inversely related to the area as well, i.e. diffusion is accelerated with decreasing area of the coating defect. Note as well that the Warburg impedance relates only to infinite diffusion, i.e. diffusion in which the possible extension of the diffusion layer is not limited, but this is a quite good approximation when dealing with diffusion in soil.

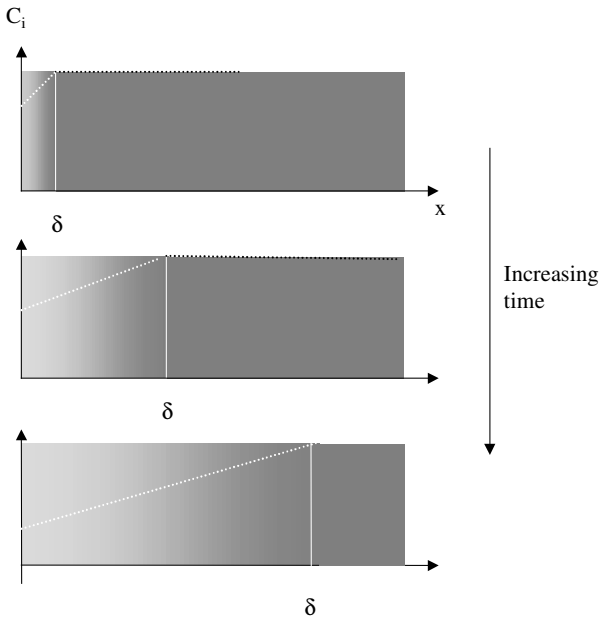

Figure 9. Schematic illustration of the concentration gradient across the diffusion layer. The diffusion layer distance as well as the surface concentration (C_i at x = 0) may vary with time.

Referring to equation (18), the flux of species related to diffusion is proportional to the difference in concentration existing across the diffusion layer, but inversely proportional to the extension or thickness of the diffusion layer. The distance δ (thickness of diffusion layer) over which the concentration difference exist may vary with time as illustrated in figure 9. Also, the surface concentration may change throughout time.

Partly derived from the diffusion equations (18) and (19), the thickness of the diffusion layer δ under steady state (DC) conditions is a function of time and the diffusion:[2]

$$\delta(t) = \sqrt{\pi \cdot D \cdot t} \tag{24}$$

Experiments involving a cathodically protected steel surface submerged in an artificial soil solution suspended in sand have shown[7] that the rate by which an alkaline front moves away from the protected surface defines a diffusion coefficient for H^+ in that suspension in the order 3.4 x 10^{-4} cm^2/sec. (tabulated values are in the order of 9 x 10^{-5} cm^2/sec (H^+ in weak acid[8]) hence the measured value may be surprisingly high).

Under alternating conditions e.g. brought about by an AC voltage having frequency f, the extension of the diffusion layer d can be described as a function of the diffusion coefficient D and the applied frequency:[2]

$$\delta(f) = \sqrt{\frac{\pi \cdot D}{2 \cdot f}} \tag{25}$$

When comparing equation (24) and (25) one important aspect is that the thickness of the diffusion layer is considerably larger in a pure DC condition (24) than the

thickness under say 50 Hz AC (25). Using the measured diffusion coefficient as an example, the thickness of the diffusion layer as a function of time becomes:

$$\delta / \mathrm{cm} = 1.97 \cdot \sqrt{\mathrm{t} / \mathrm{hours})} \tag{26}$$

This equation shows e.g. that after only 24 hours, the diffusion layer (the extension of the zone being chemically affected by CP) reaches 10 cm out into the bulk of the soil. In comparison, during a 50 Hz AC cycle, the extension of the diffusion layer is in the order of μm. In other words, during one single cycle of AC, the diffusion limitation is very modest and may be disregarded in comparison with the limiting (or modifying) effects of diffusion under long-term DC influence. This means that terms like thickness of the diffusion layer and surface versus bulk concentration are different in the DC (long term) and in the AC (short term; within one cycle) situation. If one could record exclusively the faradaic current within one cycle of AC simultaneously with the off-potential, one would expect a quite perfect charge transfer controlled Volmer-Butler curve with no effect of diffusion. The bulk concentration of the involved species would approach the surface concentration.

However, due to a rectification or a DC offset that causes a certain DC current to flow throughout time, the bulk versus surface concentration (appearing in the Volmer-Butler equation (16)) and the extension of the diffusion affected zone (as defined in figure 9) becomes important. Still, the fact that diffusion is not a limiting parameter within one cycle of AC, the faradaic current as described by a Volmer-Butler becomes a very good approximation. Throughout time however, the elements enclosed in the Volmer-Butler equation may change due to diffusion processes. In particular, this relates to exchange current density and equilibrium potentials whereas ratio between surface versus bulk concentration of involved species is expected to be around 1 even though the actual concentrations may change.

Conclusions

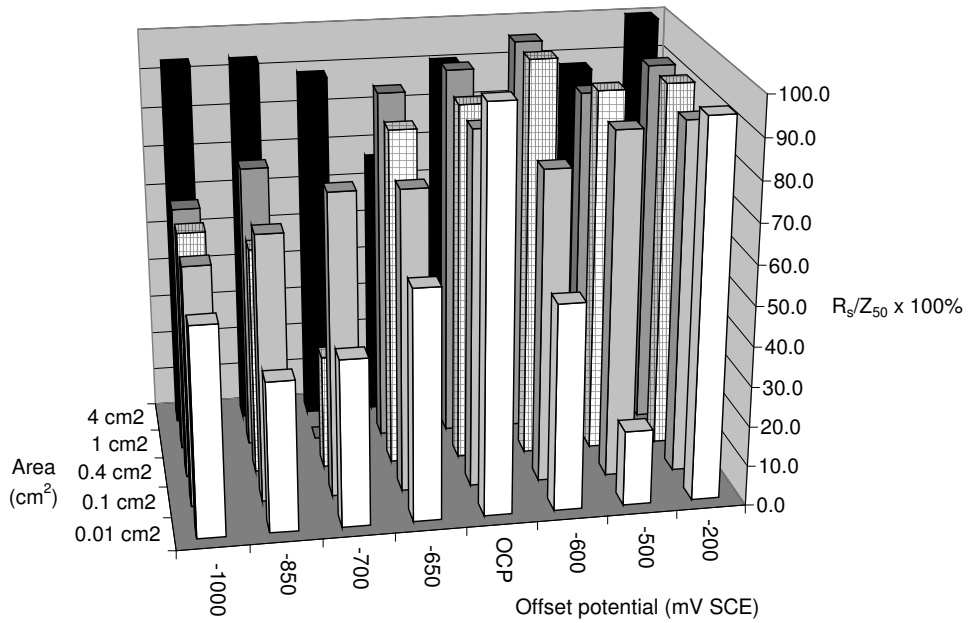

References

1. Handbuch des katodischen Korrosionsshutzen, (W.v. Baeckmann, W. Schwenk, W. Prinz, eds.), VCH Verlagsgesellschaft, Weinheim, 1989.

2. L.V. Nielsen, "Precipitation of solids from Artificial Soil Solution nearby Cathodically Protected Steel Surfaces", DONG, AC-Corrosion, (Notes on... file 10/19), November 1998.

3. "Instrumental methods in electrochemistry", (Southampton electrochemistry group, eds.), Ellis Horwood Limited, Chichester, 1985.